Monte Carlo Simulation of Head-to-Head, Tail-to-Tail Polypropylene and Its Mixing with Polyethylene in the Melt

E. Demet Akten and Wayne L. Mattice*

Institute of Polymer Science, The University of Akron, Akron, Ohio 44325-3909

Received December 5, 2000; Revised Manuscript Received February 21, 2001

ABSTRACT: Simulations have been performed at 473 K for one-component melts of polyethylene (PE) and head-to-head, tail-to-tail polypropylene (hhPP) as well as a mixture of the two species. The densities are 0.760, 0.753, and 0.756 g/cm^3 for these three *NVT* simulations, respectively. The Monte Carlo simulation uses coarse-grained representations of the chains on a sparsely occupied high coordination lattice. The short-range intramolecular interactions are controlled by rotational isomeric state models for the two types of chains, and the intermolecular interactions are represented by a discretized version of Lennard-Jones potential energy functions. Equilibrated coarse-grained replicas are reverse-mapped to atomistically detailed models in continuous space. The pair correlation functions clearly demonstrate the onset of demixing for the two-component melt, which is qualitatively consistent with the conclusion from small-angle neutron scattering reported by Jeon et al. [*Macromolecules* **1998**, *31*, 3340]. Analysis of the components of the energy in the simulations shows that the positive energy change on mixing is completely dominated by the intermolecular Lennard-Jones contributions, with negligible contributions from the short-range intramolecular interactions in the rotational isomeric state models. Quantitative comparison with experiment shows that the χ deduced from the simulations is larger than the χ deduced from the experiments. Several factors in the experiments and in the simulations may contribute to the quantitative difference.

Introduction

The miscibility of pairs of polymeric hydrocarbons is subject to strong changes as a consequence of seemingly minor adjustments in the covalent structure of the chains. The sensitivity of the mixing behavior to minor structural changes is illustrated by conventional head-to-tail polypropylene (PP), where the change from miscibility to immiscibility in the melt can be achieved by manipulating the stereochemical compositions of the two components. In the melt, isotactic polypropylene (iPP) is miscible with atactic polypropylene (aPP),[1] but syndiotactic polypropylene (sPP) demixes from either aPP or iPP.[2−4] This behavior has been reproduced qualitatively in simulations.[5,6] The more recent simulation also provides a mechanistic interpretation of the mixing behavior.[6] The melt of sPP retains a slight amount of residual structure, which is evident in pair correlation functions and in the dynamics of the chains. This residual structure is disrupted when a sPP chain is strongly diluted with iPP chains, as shown by analysis of the energetics and dynamics in the simulation. The reluctance of sPP chains to mix with either aPP or iPP chains is a consequence of their resistance to the disruption of this structure.

The behavior of the simulation of another pair of simple polymeric hydrocarbons, polyethylene (PE) and head-to-head, tail-to-tail polypropylene (hhPP), is reported here. Prior experimental work identifies this pair as being immiscible in the melt,[7] and that behavior is found also in the simulation. However, the mechanism responsible for demixing in the present simulation of hhPP/PE is found to be fundamentally different from the mechanism identified previously[6] in the simulations of aPP/sPP and iPP/sPP melts, as is evident from a decomposition of the average change in energy per bead on mixing. Quantitative agreement with the experimentally observed behavior is not achieved (χ from the simulation is larger than χ from experiment). Contributions to the quantitative disagreement, and a conceptual route to its reduction, are identified.

The simulations must confront the difficulty in equilibrating dense polymer melts, due to the long times required for a sufficiently thorough equilibration. Our approach utilizes a conventional Metropolis Monte Carlo (MC) simulation in a way that takes advantage of bridging techniques.[8] Mapping of rotational isomeric state (RIS) models onto the high coordination lattice causes the coarse-grained chains, and their component subchains, to retain the appropriate distribution of end-to-end vectors.[9,10] Intermolecular interactions are handled by an approach that has its foundation in the classical description of the second virial coefficient of a nonideal gas.[11] This combination of constraints on the short-range intramolecular conformations and long-range interactions permits the construction of a *reversible* bridge between an atomistically detailed description of the dense system in continuous space and a coarse-grained representation of the same system on the discrete space of a sparsely occupied high coordination lattice. The reversibility of the bridge denotes the ability to "reverse/map" a coarse-grained representation into a fully atomistic description of the same system.[5,12] The technique has been reviewed recently.[8,13]

Model and Method

The high coordination lattice ($10i^2 + 2$ sites in shell i) with a step length of 2.5 Å is obtained by elimination of alternate sites from a diamond lattice on which the step length was that of a C−C bond. Alternate carbon atoms are also deleted from the backbone of each chain. Each occupied site represents C_2H_4 for PE and C_3H_6 for hhPP. Occupancy of 18.1% (11.9%) of the sites for PE (hhPP) gives a density of 0.760 (0.753) g/cm^3. These occupancies were used for the simulation of the one-

10.1021/ma0020739 CCC: $20.00
Published on Web 04/07/2001

component melts. They are based on the densities reported by Orwoll for PE and iPP at the temperature of the simulation.[14] A slightly higher density, 0.771 g/cm^3, has been reported for hhPP.[15] The two-component melt, composed of 11 chains of PE and 9 chains of hhPP, had a weight fraction of hhPP of 0.55, an occupancy of 14.6% and a density of 0.756 g/cm^3. The density of the blend is taken to be the average of the densities of the two pure components. The chains were represented by 50 beads, which reverse map to $C_{100}H_{202}$ and $C_{150}H_{302}$ for PE and hhPP, respectively. The hhPP chains are atactic. The dimensions of the periodic boxes, in units of the step length of 2.5 Å, were 17 × 18 × 19 for PE, 20 × 20 × 21 for hhPP, and 18 × 19 × 20 for the mixture. The angle between any two axes is 60°.

The simulation has a mandatory prohibition of double occupany of any site on the lattice. The RIS models used for the intramolecular short-range interactions were the classic model described for PE by Abe et al.[16] and a new model for hhPP[17] that reproduces the experimentally observed[18] mean-square dimensions in the melt. Pairs of beads in the one-component melts were treated with a discretized version[11] of Lennard-Jones (LJ) potential energy functions that describe the pairwise interactions of ethylene ($\epsilon_{PE,PE}/k_B$ = 205 K, $\sigma_{PE,PE}$ = 4.2 Å)[19] and propane ($\epsilon_{hhPP,hhPP}/k_B$ = 237.1 K, $\sigma_{hhPP,hhPP}$ = 5.118 Å).[20] The discretization starts with the expression for the second virial coefficient, B_2, in terms of the Mayer f function.

$$B_2 = -{}^1/_2\int\{\exp(-u(r)/k_BT) - 1\}\,dr = -{}^1/_2\int f\,dr \quad (1)$$

This integral is rewritten as a sum of contribution from consecutive shells.

$$B_2 = (V_{cell}/2)[1 - \sum z_i\langle f\rangle_{ith}] \quad (2)$$

The z_i are the coordination numbers, $z_i = 10i^2 + 2$, and $\langle f\rangle_{ith}$ is the average of the Mayer f function over the sites in the ith shell. This average is then converted to a discrete energy for shell i, u_i.

$$\exp(-u_i/k_BT) - 1 = \langle f\rangle_{ith} \quad (3)$$

For interaction of pairs of dissimilar beads in the mixture, the pertinent values of the LJ parameters were obtained by the usual appeal to the Berthelot mixing rules.

$$\epsilon_{hhPP,PE} = (\epsilon_{hhPP,hhPP}\epsilon_{PE,PE})^{1/2} \quad (4)$$

$$\sigma_{hhPP,PE} = (\sigma_{hhPP,hhPP} + \sigma_{PE,PE})/2 \quad (5)$$

At the temperature of the simulations, 473 K, discretization of these LJ potential energy functions produces the shell energies presented in Table 1. A large positive value is obtained for u_1 because it covers distances smaller than σ. The value of u_2 is also positive, but only weakly so for PE because the pertinent LJ potential energy function has a value of σ that falls within the range of distances covered by the second shell. The strongest attraction is found in the third shell. Attractions become weaker as the shell number increases above 3. Two sets of equilibrations were performed, which differ in whether the intermolecular interactions were truncated at u_4 or u_5. Most of the results are based on the truncation at u_4; the text will clearly indicate

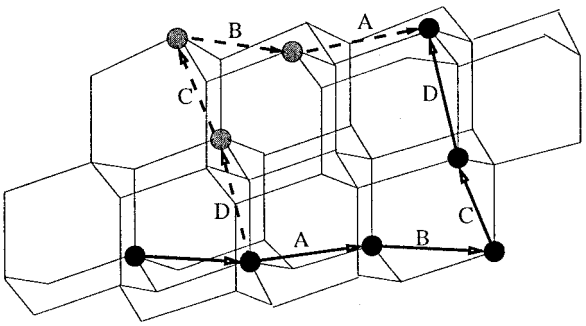

Figure 1. A three-bead local move that reverses the order of the four vectors A, B, C, and D from the set depicted by solid arrows to the set depicted by dashed arrows.

Table 1. Shell Energies (kJ/mol) Used in the Simulations at 473 K

shell	PE,PE ϵ/k_B = 205 K, σ = 4.2 Å	hhPP,hhPP ϵ/k_B = 237.1 K, σ = 5.118 Å	PE,hhPP ϵ/k_B = 220.5 K, σ = 4.659 Å
1	12.980	26.693	18.401
2	0.101	3.065	1.178
3	−0.593	−1.088	−0.879
4	−0.131	−0.464	−0.257
5	−0.034	−0.127	−0.068
6	−0.011	−0.042	−0.022
7	−0.004	−0.017	−0.009
8	−0.002	−0.007	−0.004
9	−0.001	−0.004	−0.002

when the truncation was at u_5. In a few clearly stated instances, the energetic analysis of the equilibrated structures uses additional shells.

Two types of local moves were used, along with reptation, during the simulation on the high coordination lattice. One type is the set of single-bead moves that was described earlier.[13] These moves correspond to three- or four-bond crankshaft motions in the atomistically detailed description of the chain. The other type is a set of multiple-bead local moves based on the pivot algorithm methodology.[21] The specific set used in this simulation applies an appropriate symmetry operation to a subchain consisting of 2, 3, or 4 consecutive beads in a coarse-grained chain. An illustrative example of a three-bead move is depicted in Figure 1. The single-bead moves have been demonstrated previously to produce an efficient relaxation of PE melts,[13] but hhPP relaxes much more slowly than PE, if only single bead moves are used. Incorporation of the multiple-bead moves significantly improved the rate of equilibration of the hhPP melt. The implementation of reptation was different for PE and for hhPP. For PE, reptation extracted one bead (corresponding to a C_2H_4 unit) from one end of the chain and attached it at the other end of the same chain. For hhPP, however, the extracted unit corresponded to a repeat unit of C_6H_{12}, which is represented by two consecutive beads in the coarse-grained chain. The moves avoided double occupancy of any site and also rigorously avoided the "collapse" of beads,[12] using the 12 × 12 matrix appropriate for the relationship between the high coordination lattice and its underlying diamond lattice.[10] Acceptance of a proposed move was based on the Metropolis criteria at 473 K, where the ΔE is the sum of the changes in the local intrachain (rotational isomeric state) and interchain (u_i) interactions.

In each Monte Carlo step (MCS), each chain is first subjected to an attempted reptation, and then a single-

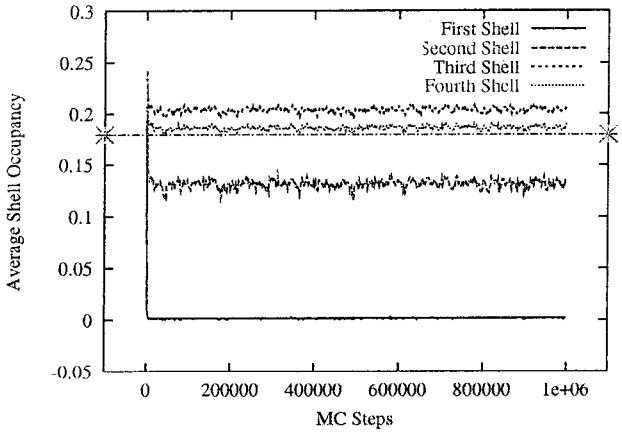

Figure 2. Initial equilibration of the average shell occupancies for the first four shells in the simulation of the PE melt at a density of 0.760 g/cm^3 and 473 K. The bulk occupancy, 0.181, is denoted by the horizontal line end-blocked with "X".

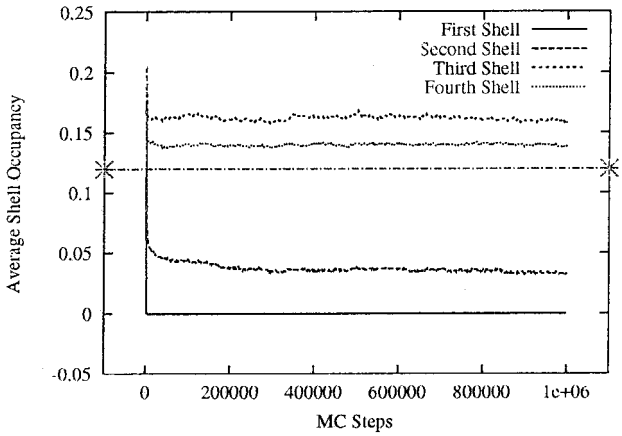

Figure 3. Initial equilibration of the average shell occupancies for the first four shells in the simulation of the hhPP melt at a density of 0.753 g/cm^3 and 473 K. The bulk occupancy, 0.119, is denoted by the horizontal line end-blocked with "X".

bead move is attempted on each bead. The single-bead moves are followed by the multiple-bead moves based on the pivot algorithm. This procedure selects a length averaging three beads at a random location along the chain and repeats the attempt 16 times. If every pivot move was accepted, 48 of the 50 beads in the chain would be moved by it during each MCS. The systems went through an initial equilibration period, which was judged to have been completed when the potential energies no longer exhibited a systematic drift. Equilibration of the occupancies of the first four shells is presented in Figures 2 and 3 for the two one-component systems. The initial equilibration was followed by the production runs, of duration 5 million MCS for PE and 20 million MCS for hhPP and for the blend.

Arbitrarily selected snapshots of the equilibrated coarse-grained chains on the high coordination lattice were reverse-mapped to atomistically detailed representations in continuous space. This procedure has two steps.[12] First, all of the covalent bonds, and all of the carbon and hydrogen atoms, are restored to the system using conventional bond lengths, tetrahedral bond angles, and the discrete space of the diamond lattice that underlies the high coordination lattice. Then the atomistically detailed structure is moved off-lattice by performing an energy minimization with the PCFF force field and software provided by Molecular Simulations, Inc. The energy minimization does not produce large-scale motions of the chains. Instead, it causes them to fall into a local energy minimum in continuous configuration space that is situated close to the starting configuration on the diamond lattice.

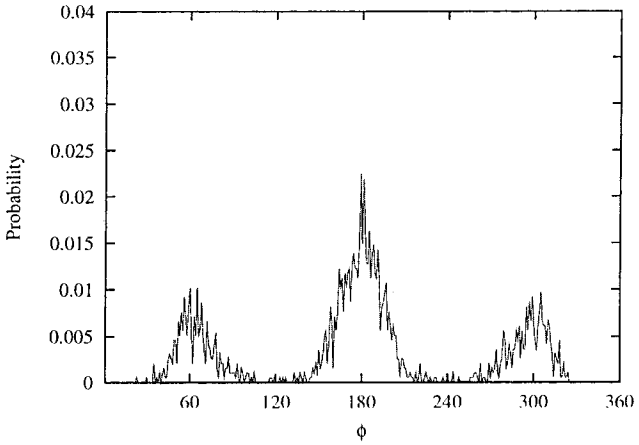

Figure 4. Distribution of torsion angles at the restored C−C bonds in the backbone of the nine hhPP chains in a reverse-mapped and energy minimized snapshot of hhPP at 473 K.

Results and Discussion

Local Structure of the Reverse-Mapped One-Component Melts. An example of the distribution of torsion angles at the restored C−C bonds in the main chain of the 20 hhPP chains in an arbitrarily selected snapshot is depicted in Figure 4. Before energy minimization, this distribution consists of delta functions located precisely at ϕ of 180° and ±60°, as required for a diamond lattice. The rotational isomeric state character of the chains is retained after energy minimization, but there is a substantial broadening of the distribution of torsion angles in each rotational isomeric state. The broadening of this distribution function is greater for hhPP than for PE (not shown here), as expected from the conformational analysis of PE by Abe et al.[16] The distribution for torsion angles for PE in the present simulation is similar to the one depicted earlier.[12] The population of the trans state is 0.52 in PE and 0.56 in hhPP, with the balance of the population equally split between the two gauche states. The displacement of the maximum population in the gauche state from ±60° is smaller for hhPP than for PE,[12] where it is about 6°, as expected from the conformational energy analysis of Abe et al.[16]

Pair correlation functions, $g(r)$, were used to characterize the intermolecular structure of the melts. Here $g(r)$ is evaluated for all pairs of carbon atoms in different chains and for all pairs of carbon atoms in the same chain that are separated by at least four bonds. Pair correlation functions for the two one-component melts, obtained as the average over seven reverse-mapped and energy-minimized snapshots, are depicted in Figure 5. For comparison, the figure also depicts the $g(r)$ obtained by a classical, all-atom molecular dynamics simulation of a melt of $C_{44}H_{90}$ at 400 K.[22] The first two maxima, and first two minima, in $g(r)$ occur at nearly the same positions in the two simulations of PE, but they are stronger in the present MC simulation of $C_{100}H_{202}$ at 473 K than for the prior MD simulation of $C_{44}H_{90}$ at 400 K. The different amplitudes may arise in part from the unequal influence of end effects in the two simulations. The $g(r)$ for the hhPP has its maxima and minima

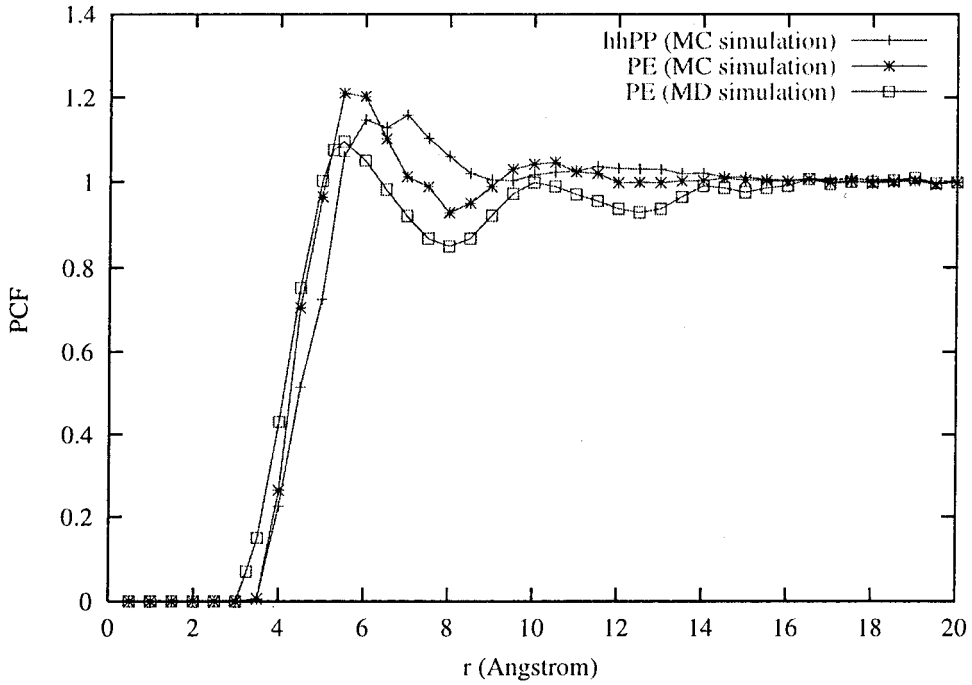

Figure 5. Pair correlation functions for the carbon atoms in reverse-mapped and energy minimized snapshots of PE ($C_{100}H_{202}$) and hhPP ($C_{150}H_{302}$) melts at 473 K, along with the pair correlation function reported by Smith et al.[20] for a MD simulation of $C_{44}H_{90}$ at 400 K.

at distinctly different values of r from those observed in either of the PE simulations. The maxima and minima are less sharply defined in hhPP than in PE. Decomposition of the $g(r)$ for carbon atoms in hhPP into various contributions (not shown here) reveals that the first maximum occurs at r as small as 4.5 Å (methyl−methyl interactions) or as large as 7 Å (backbone−backbone interactions). Since the backbone contains twice as many carbon atoms as the methyl groups, the more numerous backbone−backbone interactions determine the location of the first maximum in $g(r)$ when all carbon atoms are used in the evaluation. The less dense packing of the backbones in hhPP, induced by the pendant methyl groups, causes displacement of the strongest maximum in $g(r)$ from about 5.7 Å in PE to about 7 Å in hhPP. These differences in the $g(r)$ of PE and hhPP are qualitatively consistent with those reported by Maranas et al.[23] for molecular dynamics simulations at 423 K of models represented by 66 (PE) or 31 (hhPP) united atoms, with one united atom per carbon atom.

The solubility parameters for the one-component melts can be evaluated directly from the coarse-grained configurations on the high coordination lattice or from the reverse-mapped and energy-minimized structures. When the evaluation is performed using the coarse-grained chains, the result is strongly affected by the cutoff for u_i in the analysis of the snapshots, even when the same cutoff (at u_4) is used for the MC simulation that produces the snapshots. The influence of the upper limit for the u_i in the analysis is depicted in Figure 6. The estimate of the solubility parameter increases as more of the long attractive tail of the LJ potential energy function is included, by increasing the upper limit for i in the shells used in the analysis. A limiting value has not been obtained even when truncation is delayed until u_9. A hypothetical extension of the truncation to infinity would appear to yield a solubility parameter near 8 (cal/cm^3)$^{1/2}$, or 68 (J/cm^3)$^{1/2}$, for coarse-grained hhPP, based on plausible extrapolation of the curve in Figure 6. This limit is close to the lower end of the experimental range of 8.2−9.2 (cal/cm^3)$^{1/2}$, or 70−79 (J/cm^3)$^{1/2}$.[24] Table 2 presents solubility parameters calculated from the coarse-grained models, using either four or nine shells in the analysis of 1000 coarse-grained snapshots, along with the results obtained with the MSI software (Insight II) using seven reverse-mapped and energy-minimized snapshots.

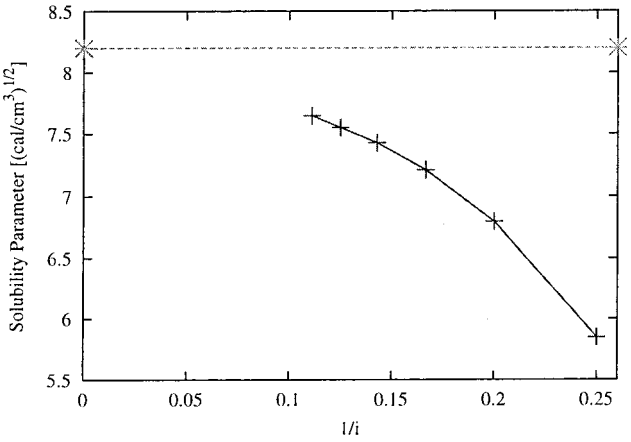

Figure 6. Estimate of the solubility parameter for coarse-grained hhPP melts at 473 K and a density of 0.753 g/cm^3, as a function of the i for the last shell energy, u_i, used in the analysis. The horizontal dashed line is the lower limit of the range of 8.2−9.2 (cal/cm^3)$^{1/2}$, or 70−79 (J/cm^3)$^{1/2}$, tabulated by van Krevelen and Hoftyzer.[21]

Table 2. Average Solubility Parameters, (J/cm^3)$^{1/2}$, and Standard Deviation for 1000 Coarse-Grained and Seven Atomistically Detailed Snapshots

	PE	hhPP
coarse-grained, 4 shells	52.6 ± 0.0	50.1 ± 0.0
coarse-grained, 9 shells	58.6 ± 0.0	65.5 ± 0.0
fully atomistic	64.8 ± 0.5	57.0 ± 0.0
experimental (ref 24)	66−71	70−79

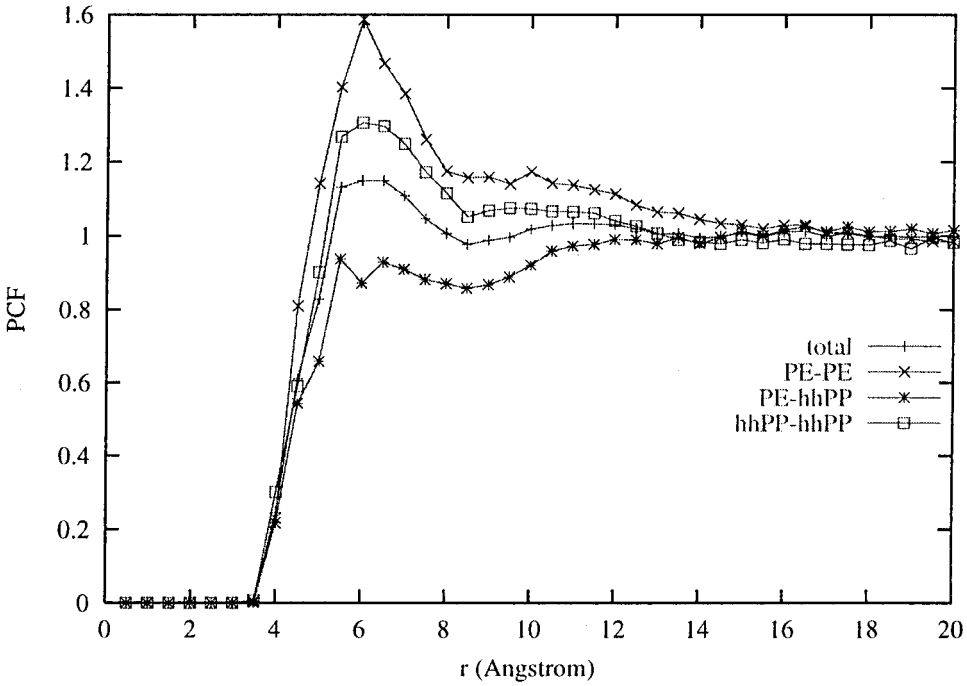

Figure 7. Pair correlation functions for atomistically detailed representations of the mixture of PE and hhPP at 473 K and a density of 0.756 g/cm^3, using truncation at u_4 during the MC simulation of the coarse-grained chains.

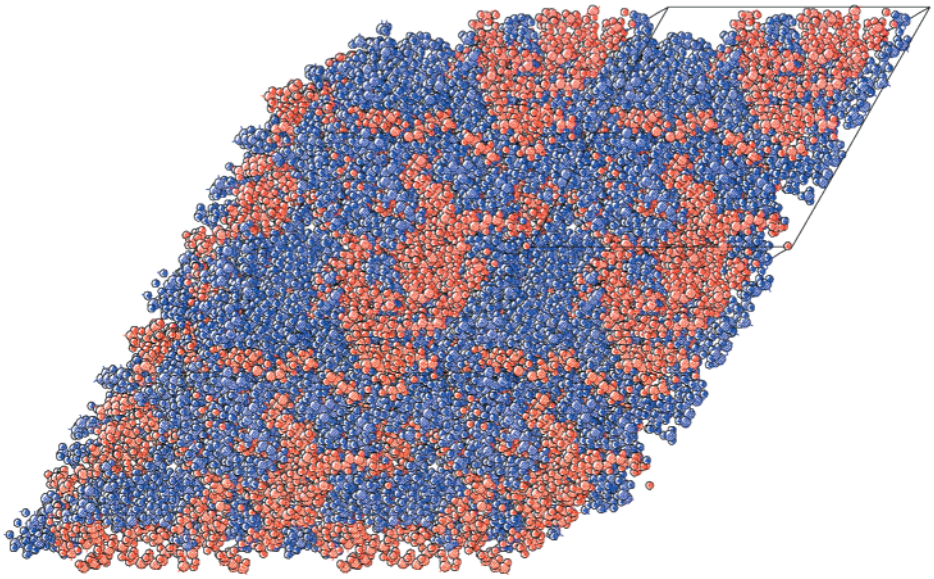

Figure 8. An illustrative shapshot of the mixture of PE (blue) and hhPP (red) chains at 473 K and 0.756 g/cm^3, after reverse-mapping and energy minimization.

Analysis of the Blend and the Miscibility of PE with hhPP. Figure 7 depicts four distinguishable $g(r)$ for the blend, based on equilibration of the coarse-grained models with truncation at u_4, followed by reverse-mapping and energy minimization of seven independent snapshots. The total $g(r)$ has features similar to the average of the $g(r)$'s for the two pure components in Figure 5. Therefore, the overall distribution of the carbon atoms in the mixture, as revealed by the total $g(r)$, is unremarkable.

Decomposition of the total $g(r)$ into its components reveals that the mixture is not homogeneous. The carbon atoms in the two individual components of the mixture each exhibit a stronger first maximum for their $g(r)$ in the mixture (Figure 7) than in their one-component melts (Figure 5). More importantly, the $g(r)$ arising from the cross-correlation of carbon atoms in PE with carbon atoms in hhPP lies below the other three $g(r)$ in Figure 7 for separations of 4−12 Å. This result shows that the carbon atoms in different types of chains tend to avoid intimate interaction with one another, on a distance scale of about 10 Å or less. The carbon atoms prefer instead to interact closely with carbon atoms from another chain of the same kind. The decomposition of the total $g(r)$ into its components demonstrates that the mixture is on the verge of separation into two phases. A pictorial representation of the mixture is presented in Figure 8, based on one of the reverse-mapped and energy-minimized snapshots. The immiscibility inferred for this system from the simulation is qualitatively consistent with the behavior observed experimentally.[7]

Table 3 presents the average energy per coarse-grained bead, along with its decomposition into the two components arising from the short-range intramolecular

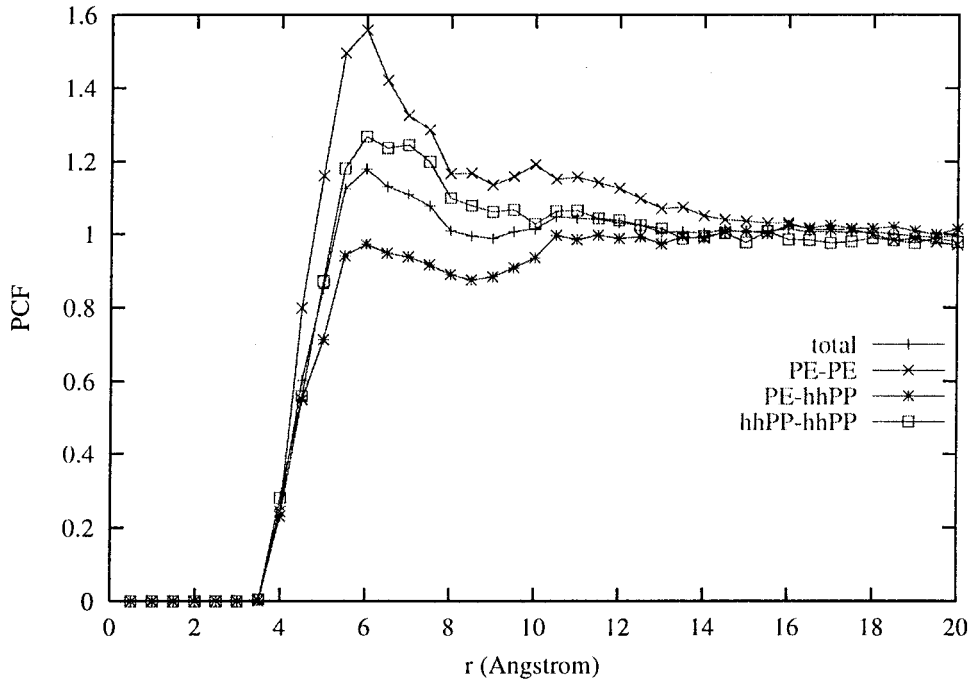

Figure 9. Pair correlation functions for atomistically detailed representations of the mixture of PE and hhPP at 473 K and a density of 0.756 g/cm^3, using truncation at u_5 during the MC simulation of the coarse-grained chains.

Table 3. Average Energy (kJ/mol) per Coarse-Grained Bead and the Contributions to the Average from the Rotational Isomeric State Model and the Lennard-Jones Interactions; Standard Deviations Are for 1000 Replicas

system	total	RIS (PE)	RIS (hhPP)	LJ
pure PE	-1.585 ± 0.001	7.058 ± 0.001		-8.644 ± 0.001
pure hhPP	-11.881 ± 0.002		5.748 ± 0.002	-17.629 ± 0.002
mixture	-5.796 ± 0.003	7.059 ± 0.001	5.802 ± 0.004	-12.288 ± 0.003

interactions in the rotational isomeric state models and the intermolecular interactions and long-range intramolecular interactions represented by the discretized LJ potential energy functions. The average LJ energy is negative, as expected for a cohesive system. The positive value for the average of the RIS energy arises from the arbitrary choice of a zero for this energy, and no special significance should be attributed to its sign. It is appropriate to compare the RIS energy for the same chain in the two different environments. The RIS contribution per bead for PE is virtually identical in its one-component melt and in the mixture, and the RIS contributions per bead for hhPP are nearly identical in these two situations. This behavior is consistent with a similar distribution of conformations for each chain in its one-component melt and in the mixture.

The information contained in Table 3 can be used to calculate the average change in energy per bead upon mixing of the chains. This change is positive, $\Delta E_{\text{total}} = 0.422 \pm 0.004$ kJ/mol, which is consistent with the conclusion from the $g(r)$ in Figure 7 that the mixture is on the verge of phase separation. Decomposition of ΔE_{total} into its two components shows that it is dominated by the contribution from the LJ interactions, $\Delta E_{\text{LJ}} = 0.400 \pm 0.004$ kJ/mol and $\Delta E_{\text{RIS}} = 0.024 \pm 0.004$ kJ/mol. The short-range intramolecular interactions contribute only about 6% of ΔE_{total}. In good approximation, the energetic change on mixing can be estimated from the intermolecular interactions alone. This energetic origin of the immiscibility of PE with hhPP is qualitatively different from the origin of the immiscibility of sPP with either aPP or iPP in the melt.[6] For sPP/aPP and sPP/iPP melts, ΔE_{RIS} and ΔE_{LJ} make nearly equal contributions to the positive ΔE_{total}. The sPP prefers a different distribution of local conformations in its own melt and in the mixtures, and the change in this distribution of conformations makes a significant contribution to ΔE_{total}.[6] With PE/hhPP, on the other hand, the chains have very nearly the same distribution of conformations in their one-component melts and in the mixture, and ΔE_{total} receives a negligible contribution from ΔE_{RIS}.

Quantitative Comparison with Experiment. The immiscibility of PE/hhPP in the melt inferred from the simulation is qualitatively consistent with experimental results. It is of interest to see how far a quantitative comparison can be pushed and identify factors that may influence this comparison.

The experiments were performed with materials that were hydrogenated or deuterated polymers obtained from anionically polymerized 1,3-butadiene or 2,3-dimethyl-1,3-butadiene.[7] Small-angle neutron scattering measurements up to 440 K, with the two different choices for the component that is deuterated, yield

$$\chi_{\text{hPE/dhhPP}} = -0.0276 + 17.56/T \quad (6)$$

$$\chi_{\text{dPE/hhhPP}} = -0.0311 + 17.50/T \quad (7)$$

When extrapolated an additional 33 K above the upper temperature covered in the experiments, these equations give a χ of about 0.01 at the temperature of the simulation, 473 K. The simulation described above produces a value of $\Delta E_{\text{LJ}}/k_{\text{B}}T$ that is nearly an order of magnitude larger, 0.09 ± 0.00. Several factors may contribute to the quantitative disagreement.

The samples studied in the experiment and in the simulation are not precisely the same. The anionic

polymerization of the dienes did not proceed entirely by 1,4 addition but instead had a small amount (7% for 1,3-butadiene, 5% for 2,3-dimethyl-1,3-butadiene) of 1,2 addition. Hydrogenation or deuteration thereby produces a low content of ethyl branches in the PE and a low content of backbone carbon atoms in hhPP that bear both an isopropyl and a methyl branch. No such irregularities in covalent structure were present in the simulation. On the other hand, the chains were of higher molecular weight (by factors of 5 for PE and 7 for hhPP) in the experiment than in the simulation, and therefore the simulation is more vulnerable to end effects.

Since the ΔE_{total} in the simulation is dominated by ΔE_{LJ}, small changes in the LJ parameters selected as the input for the simulation of the one-component melts, or replacement of the 6−12 form of this potential energy function by a softer 6−9 potential form, might affect the quantitative comparison between simulation and experiment. More subtlely, even a slight deviation of the system from precise adherence to the usual Berthelot mixing rules, eqs 4 and 5, would certainly affect ΔE_{LJ}.

Even if the input LJ parameters, form of the LJ potential, and the Berthelot mixing rules are precisely correct, the quantitative comparison might still be at the mercy of the shell number selected for truncation of the LJ potential during the Monte Carlo simulation. There is a strong temptation to truncate the LJ potential early, because the calculation of the long-range interaction is the most time-consuming part of the simulation. If t_i denotes the time required for 1 MCS when the intermolecular interactions are truncated at shell i, t_3, t_4, ..., t_9 are in the ratio 1:2.1:3.8:6.3:9.7:14.1:19.6.

To investigate the possibility that truncation affects the quantitative comparison with experiment, the MC simulations described above were repeated with truncation at u_5 rather than u_4. The $g(r)$ for the mixture are presented in Figure 9. Comparison with Figure 7 shows that the change in truncation does not affect qualitative conclusions, because at first glance the figures appear to be identical. If the objective of the simulation was simply a qualitative assignment of the mixture as miscible or immiscible, the extra time spent in the simulation with truncation at u_5, instead of u_4, was time wasted.

However, a more careful inspection of the two figures reveals subtle differences. These differences are apparent as a tendency for a smoothing in Figure 9 of some of the rougher features seen in the $g(r)$ in Figure 7. This change can be seen at 6−10 Å in the pairs of $g(r)$. These subtle changes in the $g(r)$ produce small changes in the average energy per bead. The value of ΔE_{total} is sensitive to these small changes, because ΔE_{total} is obtained as a small difference between large numbers. There is a reduction in ΔE_{total} from 0.422 ± 0.004 kJ/mol with truncation at u_4 to $\Delta E_{\text{total}} = 0.349 \pm 0.006$ kJ/mol when truncation is extended to u_5. Virtually all of this change arises from ΔE_{LJ}, as expected. The estimate of χ from the simulation decreases by 20% with the change in truncation. This change moves the estimate from simulation in the direction indicated by the experiment.[7] We have not investigated whether this change in the estimate of χ would persist if additional simulations were performed with truncation at successively higher shell numbers.

Conclusion

Pair correlation functions evaluated from simulation of systems composed of coarse-grained chains show that PE and hhPP are on the verge of phase separation in the melt at 473 K. Both types of chains have a similar distribution of conformations in the mixture and in their one-component melts. The phase separation is driven by intermolecular interactions, with a negligible contribution from short-range intramolecular interactions. Therefore, the phase separation of PE and hhPP arises for fundamentally different reasons than the phase separation seen in mixtures of sPP with either aPP or iPP. Changes in the truncation of the discretized LJ potential energy function in the simulation do not produce qualitative changes in the pair correlation functions. However, they do produce subtle changes which may be sufficient to affect the quantiative agreement between the simulation and a χ obtained from experiment.

Acknowledgment. This research was supported by National Science Foundation Grant DMR 9844069.

References and Notes

(1) Lohse, D. J. *Polym. Eng. Sci.* **1986**, *26*, 1500.
(2) Thomann, R.; Kressler, J.; Setz, S.; Wang, C.; Mülhaupt, R. *Polymer* **1996**, *37*, 2627.
(3) Thomann, R.; Kressler, J.; Rudolf, B.; Mülhaupt, R. *Polymer* **1996**, *37*, 2635.
(4) Maier, R. D.; Thomann, R.; Kressler, J.; Mülhaupt, R.; Rudolf, B. *J. Polym. Sci., Part B* **1997**, *35*, 1135.
(5) Haliloglu, T.; Mattice, W. L. *J. Chem. Phys.* **1999**, *111*, 4327.
(6) Clancy, T. C.; Pütz, M.; Weinhold, J. D.; Curro, J. G.; Mattice, W. L. *Macromolecules* **2001**, *34*, 9452.
(7) Jeon, H. S.; Lee, J. H.; Balsara, N. P.; Newstein, M. C. *Macromolecules* **1998**, *31*, 3340.
(8) Baschnagel, J.; Binder, K.; Doruker, P.; Gusev, A. A.; Hahn, O.; Kremer, K.; Mattice, W. L.; Müller-Plathe, F.; Murat, M.; Paul, W.; Santos, S.; Suter, U. W.; Tries, V. *Adv. Polym. Sci.* **2000**, *152*, 41.
(9) Rapold, R. F.; Mattice, W. L. *Macromolecules* **1996**, *29*, 2457.
(10) Haliloglu, T.; Mattice, W. L. *J. Chem. Phys.* **1998**, *108*, 6989.
(11) Cho, J.; Mattice, W. L. *Macromolecules* **1997**, *30*, 637.
(12) Doruker, P.; Mattice, W. L. *Macromolecules* **1997**, *30*, 5520.
(13) Doruker, P.; Mattice, W. L. *Macromol. Theory Simul.* **1999**, *8*, 463.
(14) Orwoll, R. A. In *Physical Properties of Polymers Handbook*; Mark, J. E., Ed.; American Institute of Physics: Woodbury, NY, 1996; p 81.
(15) Krishnamoorti, R. Ph.D. Dissertation, Princeton, 1994.
(16) Abe, A.; Jernigan, R. L.; Flory, P. J. *J. Am. Chem. Soc.* **1966**, *88*, 631.
(17) Akten, E. D.; Mattice, W. L.; Suter, U. W. In *Simulation Methods for Modeling Polymers*; Kotelyanski, M., Theodorou, D. N., Eds.; Marcel Dekker: in press.
(18) Graessley, W. W.; Krishnamoorti, R.; Reichart, G. C.; Balsara, N. P.; Fetters, L. J.; Lohse, D. J. *Macromolecules* **1995**, *28*, 1260.
(19) Hirschfelder, J. O.; Curtiss, C. B.; Bird, R. B. *Molecular Theory of Gases and Liquids*; Wiley: New York, 1954.
(20) Reid, R. C.; Prausnitz, J. M.; Poling, B. E. *The Properties of Gases and Liquids*; McGraw-Hill: New York, 1987.
(21) Clancy, T. C.; Webber, S. E. *Macromolecules* **1995**, *28*, 2561.
(22) Smith, G. B.; Yoon, D. Y.; Zhu, W.; Ediger, M. D. *Macromolecules* **1994**, *27*, 5563.
(23) Maranas, J. K.; Kumar, S. K.; Debenedetti, P. G.; Graessley, W. W.; Mondello, M.; Grest, G. S. *Macromolecules* **1998**, *31*, 6998.
(24) Van Krevelen, D. R.; Hoftyzer, P. J. *Properties of Polymers: Their Estimation and Correlation with Chemical Structure*; Elsevier: New York, 1976.

MA0020739